

THE GALAXY LUMINOSITY FUNCTIONS DOWN TO $M_R = -10$ IN THE COMA CLUSTER¹

HITOMI YAMANOI², YUTAKA KOMIYAMA^{2,3}, MASAFUMI YAGI², SADANORI OKAMURA⁴, MASANORI IYE^{2,3}, NOBUNARI KASHIKAWA^{2,3}, TADAFUMI TAKATA^{3,5}, HISANORI FURUSAWA⁵, MICHITOSHI YOSHIDA⁶

ACCEPTED TO AJ: *May 23, 2012*

ABSTRACT

We derived the luminosity function (LF) of dwarf galaxies in the Coma Cluster down to $M_R = -10$ at three fields located at the center, intermediate, and outskirts. The LF ($-19 < M_R < -10$) shows no significant differences among the three fields. It shows a clear dip at $M_R \sim -13$, and is composed of two distinct components of different slopes; the bright component with $-19 < M_R < -13$ has a flatter slope than the faint component with $-13 < M_R < -10$ which has a steep slope. The bright component ($-19 < M_R < -13$) consists of mostly red extended galaxies including few blue galaxies whose colors are typical of late-type galaxies. On the other hand, the faint component ($-13 < M_R < -10$) consists of largely PSF-like compact galaxies. We found that both these compact galaxies and some extended galaxies are present in the center while only compact galaxies are seen in the outskirts. In the faint component, the fraction of blue galaxies is larger in the outskirts than in the center. We suggest that the dwarf galaxies in the Coma Cluster, which make up the two components in the LF, are heterogeneous with some different origins.

Subject headings: galaxies: clusters: individual: Coma Cluster (Abell 1656) — galaxies: luminosity function — galaxies: dwarf

1. INTRODUCTION

The galaxy luminosity function (LF) is a useful measure to describe fundamental statistical properties of galaxy populations and serves as a clue to study the history of galaxy formation and evolution. Since the monumental work of the LF by Sandage et al. (1985), relatively bright part of the LF has been studied extensively both for cluster galaxies (e.g., Popesso et al. 2005) and for field galaxies (e.g., Blanton et al. 2003). However, our knowledge of the faint part of the LF ($M_R > -19$), which is dominated by dwarf galaxies, is still very limited. This is due to the difficulty in determining the distance of a large number of intrinsically faint galaxies. Published results of the faint part of the LF, especially, those of the faintest part ($M_R > -13$) remain scarce.

Clusters of galaxies are a good target to investigate the faint end of the LF because some statistical methods can be applied to identify member galaxies. In this study we chose the Coma cluster in order to investigate the faint part of the LF, that is, to study properties of dwarf galaxies and their possible dependence on different environments in this cluster. The Coma Cluster (Abell

1656) at $z = 0.023$ (Struble & Rood 1999) is the richest cluster of galaxies in the local Universe. The virial radius (r_{200}) of this cluster is $2.0 h^{-1}$ Mpc, which corresponds to a virial mass of $1.9 \times 10^{15} h^{-1} M_{\odot}$ as estimated from a weak lensing measurement (Kubo et al. 2007). It is relatively easy to take deep images of this nearby cluster which enables us to reach the faintest part of the LF.

The LF of the Coma Cluster was studied by many authors (e.g., Bernstein et al. 1995; Biviano et al. 1995; Secker et al. 1997; Trentham 1998; Adami et al. 2000; Andreon & Cuillandre 2002; Beijersbergen et al. 2002; Mobasher et al. 2003; Milne et al. 2007; Adami et al. 2008, 2009). Several techniques were used to construct the Coma LF. The statistical background/foreground subtraction is historically the main one (e.g., Bernstein et al. 1995; Trentham 1998; Andreon & Cuillandre 2002; Beijersbergen et al. 2002; Milne et al. 2007). Others include the spectroscopic redshift technique (e.g., Adami et al. 2000; Mobasher et al. 2003; Adami et al. 2009), photometric redshift technique (e.g., Adami et al. 2008) and color magnitude relation technique (e.g., Biviano et al. 1995; Secker et al. 1997). The faint-end slope of the LF derived from previous studies do not agree with each other and it seems that it depends on the magnitude ranges where the slope was measured, i.e., the slope is flatter at brighter magnitudes, and it becomes steeper at fainter magnitudes. However, a simple comparison of the values of the slope may be inappropriate because of the difference in the observed area and galaxy sampling criteria among previous studies. Most previous studies observed the cluster core only, with a few probed outskirts as well as the core.

The aim of the present study is to investigate the behavior of the faint part, especially, the faintest part of the LF of Coma cluster using a statistically significant

Electronic address: yamanoi.hitomi@nao.ac.jp

¹ Based on data collected at Subaru Telescope, which is operated by the National Astronomical Observatory of Japan

² Optical and Infrared Astronomy Division, National Astronomical Observatory of Japan, 2-21-1, Osawa, Mitaka, Tokyo 181-8588, Japan

³ Department of Astronomical Science, School of Physical Sciences, The Graduate University for Advanced Studies (Sokendai), National Astronomical Observatory of Japan, 2-21-1, Osawa, Mitaka, Tokyo 181-8588, Japan

⁴ Faculty of Science and Engineering, Hosei University, 3-7-2 Kajino-cho, Koganei, Tokyo 184-8584, Japan

⁵ Astronomy Data Center, National Astronomical Observatory of Japan, 2-21-1, Osawa, Mitaka, Tokyo 181-8588, Japan

⁶ Hiroshima Astrophysical Science Center, Hiroshima University, 1-3-1, Kagamiyama, Higashi-Hiroshima, Hiroshima 739-8526, Japan

large sample constructed from deep and wide photometric images obtained with the Subaru Suprime-Cam. Our imaging data cover much wider area than most of the previous studies that reached similar limiting magnitudes. We employ a careful procedure for subtracting the background galaxy population statistically to derive the LF of the cluster galaxy population.

We investigate the properties of the very faint dwarf population and their possible environmental dependence, if any, in terms of LF, color, and surface brightness. Our galaxy catalogs for the core and the outer areas are constructed by using the same instrument, same filters, and the same selection criteria, which ensures coherent and homogeneous photometric data to allow credible comparisons of galaxy properties in different environments of the cluster.

We adopt the standard cosmology model with $H_0 = 70$ $\text{km s}^{-1} \text{Mpc}^{-1}$, $\Omega_m = 0.3$, and $\Omega_\Lambda = 0.7$. Magnitudes are on the AB system. We assume a distance to the Coma Cluster of 100 Mpc and a distance modulus of 35.0 throughout this paper.

2. OBSERVATIONS AND DATA

2.1. Imaging Data

We perform *B*- and *R*-band observations with Suprime-Cam (Miyazaki et al. 2002) mounted on the Subaru Telescope (Iye et al. 2004) for a total of three nights, between 12 and 14 May 2007. Observing conditions were mediocre due to the occasional cloud traversals on all three nights. The Suprime-Cam covers a $34' \times 27'$ field of view with a pixel scale of $0''.202 \text{ pixel}^{-1}$. A typical seeing size was $\sim 0''.8$ in *B*- and *R*-band. We selected three fields in the Coma Cluster for the present study, and they are hereafter referred to as the Coma 1, Coma 2, and Coma 3 fields, respectively. The Coma 1 field is located in the central region of the Coma Cluster. Coma 2 is located at 1.3 Mpc projected distance to the southwest of the cluster core, in the postulated infalling region (Biviano et al. 1996; Neumann et al. 2001). Coma 3 is about 1.8 Mpc away from the cluster core, i.e., the outskirts. Figure 1 shows the three observed fields on the digitized sky survey (DSS) image. The distribution of X-ray emission is shown in Figure 2. We summarize the details of observation of the Coma Cluster in Table 1.

2.2. Control Field

In order to obtain the intrinsic LF of cluster galaxies, we must correct for the effect of contaminant galaxies, which are mainly located behind the cluster. To estimate the number of contaminant foreground and background galaxies, we use the Subaru Deep Field (SDF; Kashikawa et al. 2004)⁷ as the control field, which is located near the North Galactic Pole. The SDF was carefully chosen to avoid bright stars, bright galaxies, and nearby clusters. This field was observed with Suprime-Cam and multi-band data based on the common seeing size of $\sim 0''.98$ are available. We use the *B*- and *R*-band data taken from the SDF archive. Their filter sets are identical to those we used for the Coma Cluster. SDF data reach much deeper limiting magnitudes than the Coma data.

⁷ <http://soaps.nao.ac.jp/sdf/Project.html>

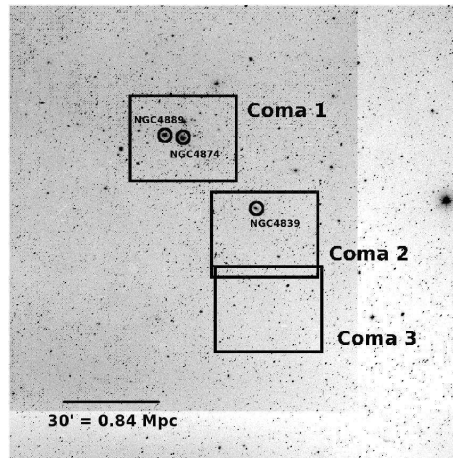


FIG. 1.— Digitized Sky Survey (DSS) (1st) image of the Coma Cluster. North is up, and East is to the left. The rectangles show the Coma 1 (center), Coma 2 (NGC 4839 groups), and Coma 3 (outskirt) fields. The three giant elliptical galaxies are marked with circles, NGC 4889, NGC 4874 and NGC 4839.

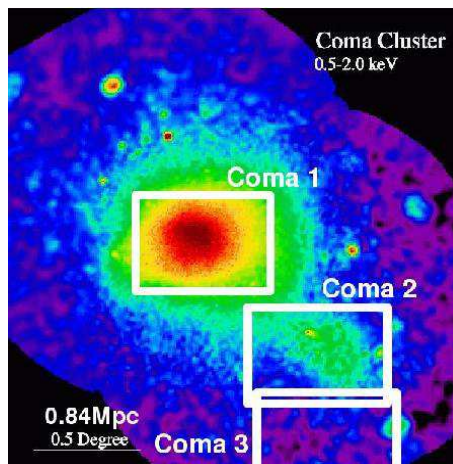


FIG. 2.— ROSAT X-ray image of the intracluster gas in the Coma Cluster from NASA HEASARC. North is up, and East is to the left. The color scale shows higher X-ray intensity for red and lower one for blue.

We consider that the population of Galactic stars in the SDF is similar to that in the Coma Cluster because the two fields have almost the same Galactic latitude ($b \sim 88^\circ$ for Coma, $b \sim 83^\circ$ for SDF). Accordingly, we use the SDF data to correct for the effect of Galactic stars in $R > 22$ where we do not apply star/galaxy separation.

We also use the imaging data of the Subaru XMM-Newton Deep Survey fields (SXDS; Furusawa et al. 2008)⁸ to examine the effect of the cosmic variance (see §4.3 for details). The SXDS fields are also observed with Suprime-Cam and the same photometric calibrations as the SDF was applied.

3. DATA REDUCTION AND CATALOG

3.1. Data Reduction

Data reduction was carried out in a standard procedure using the reduction software for Suprime-Cam; SDFRED (Yagi et al. 2002a; Ouchi et al. 2004) and Image Reduction and Analysis Facility (IRAF). We perform the

⁸ <http://www.naoj.org/Science/SubaruProject/SDS/datapolicyJ.html>

Region	Date	R.A. (J2000.0)	Dec. (J2000.0)	Band	Exp. Times (min)	Lim. Mag. (5σ)	Effective Area (arcmin ²)
Coma 1	12 Mar. 2007	12 ^h 59 ^m 46 ^s	+27°54′02″	<i>B</i>	60	26.0	769
	13-14 Mar. 2007			<i>R</i>	35	25.9	
Coma 2	12 Mar. 2007	12 ^h 57 ^m 22 ^s	+27°20′02″	<i>B</i>	60	26.5	880
	12-13 Mar. 2007			<i>R</i>	90	25.9	
Coma 3	12 Mar. 2007	12 ^h 57 ^m 23 ^s	+26°53′09″	<i>B</i>	60	26.3	863
	12-14 Mar. 2007			<i>R</i>	114	26.3	

TABLE 1
LIST OF THE OBSERVATIONS FOR THE COMA CLUSTER.

point spread function (PSF) equalization by convolving gaussians to the reduced Coma images in order to match their PSF size (FWHM) to that of the SDF image. The resulting PSF size is 4.9 pixels (0.''98) in all the images, which correspond to ~ 0.45 kpc at the distance of the Coma Cluster.

3.2. Photometric Calibration

First, we carry out an initial estimation of the photometric zero point using previous photometric catalog of Mobasher et al. (2001) and Komiyama et al. (2002), whose observations cover our target fields. However, passbands are slightly different between their catalog and our data. In order to improve the accuracy of the zero point, we re-estimate it using the photometric stars from the Sloan Digital Sky Survey (SDSS) DR7 photometric catalog which covers the Coma Cluster and the SDF. This calibration method is similar to the one by Yagi et al. (2010). Photometric zero points of all the images are corrected to give the measured counts (ADU) consistent with the stellar spectral energy distributions (SEDs) given in the Bruzual–Persson–Gunn–Stryker Atlas⁹ which is an extension of the Gunn–Stryker Atlas (Gunn & Stryker 1983). We select the stars that are detected in both the SDSS and the Suprime-Cam, and compare the stellar sequences from our data and the Gunn & Stryker’s SED in the two color planes shown in Figure 3. Red lines represent the best fits to the Gunn & Stryker’s stars. Dashed-dotted lines show the best fit to our raw data for stars brighter than $r = 21$, which are calibrated based on the initial estimation of zero points. The typical number of stars used for the calibration is about 80 and 30 in the Coma Cluster and the SDF, respectively. We correct for these offsets in the zero points by shifting our stellar sequence to the model sequence computed by convolving the Gunn & Stryker’s SEDs with the filter response curves. The offset value is mostly due to the difference of the filter response between the Suprime-Cam passbands and the filters used in Mobasher et al. (2001) and Komiyama et al. (2002). Specifically, we give the offset values; -0.28, -0.36 and -0.23 mag in *B*-band, -0.07, -0.08 and -0.11 mag in *R*-band of Coma 1, 2 and 3. The errors in the final photometric zero points are less than 0.02 mag and 0.03 mag for the Coma Cluster and the SDF images, respectively.

The Galactic extinction is corrected using the extinction map by Schlegel et al. (1998). Table 2 lists the photometric zero points and the Galactic extinction in each band.

Region	Band	zp (mag/ADU)	Galactic Extinction (mag)
Coma 1	<i>B</i>	33.04	0.041
	<i>R</i>	31.84	0.025
Coma 2	<i>B</i>	33.85	0.041
	<i>R</i>	32.66	0.025
Coma 3	<i>B</i>	34.23	0.042
	<i>R</i>	32.94	0.026
SDF	<i>B</i>	34.69	0.078
	<i>R</i>	34.26	0.048

TABLE 2
LIST OF THE PHOTOMETRIC ZERO POINTS AND THE GALACTIC EXTINCTION FOR THE COMA CLUSTER AND THE SDF.

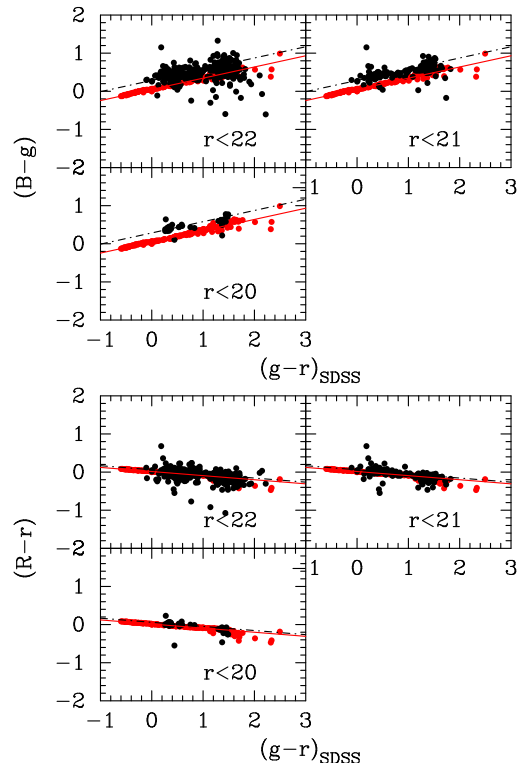


FIG. 3.— Color-color plots for stellar objects in the Coma 1 field with the initial calibration (*black dots*). The dot-dashed lines are the least square fit to stars brighter than $r = 21$ and $g - r < 1.0$ whose $B - g$ and $R - r$ are calculated from our Suprime-Cam measurements and SDSS catalog. The colors of Gunn & Stryker’s stars calculated with the filter models are plotted as red points. Red lines are the least squares fit to model stars at the range of $g - r < 1.0$.

⁹ <http://www.stsci.edu/hst/observatory/cdbs/bpgs.html>

3.3. Object Extraction and Catalog

We perform object detection and photometric measurement using the SExtractor (Bertin & Arnouts 1996) in double-image mode with the R -band image as the detection image. We identify as an object more than five connected pixels above 1.5σ of the sky background noise. We adopt `MAG_AUTO` for the total magnitudes and $2''$ circular aperture magnitudes for colors.

The limiting magnitude is derived by the method similar to that in Ouchi et al. (2004). We measure the sky counts in a number of $2''$ apertures which are distributed at random on the image, and obtain the 1σ noise by fitting a Gaussian function to the histogram of the sky counts. We confirm that there is no failure of a $2''$ aperture photometry of detected objects in the R -band and that measurements of B -band aperture magnitude of the object brighter than the limiting magnitude are successful in double-image mode. The 5σ limiting magnitudes and the effective areas are summarized in Table 1. The limiting magnitude in each band is found to be ~ 26 mag (5σ). Regions around bright stars and giant galaxies (for example, NGC 4889, NGC 4874, NGC 4898, NGC 4865, NGC 4911 and IC 4051 in the Coma 1), where the detection of faint objects fails, are masked out.

The star/galaxy discrimination is performed for objects with $R \leq 22$. We regard the objects as galaxies which are significantly more extended (FWHM > 5.6 pixels = $1.''13$) than stars (FWHM = 4.9 pixels = $0.''98$) as shown in Figure 4. As for stellar objects fainter than $R = 22$, the statistical subtraction (for details in §4.2) is applied in the following analysis. We confirm that the LFs remains unchanged if we change the star/galaxy discrimination limits to $R = 21$ or $R = 23$ instead of $R = 22$. Details are given in §5.1. We investigate the contamination from globular clusters fainter than $R = 22$ in detail in §4.4, and it is found to be negligible.

We evaluate the effective surface brightness of the objects (μ_e) in units of mag arcsec^{-2} . It is defined by the mean surface brightness inside the effective radius (radius in which half the total flux is emitted) and contains some information on the luminosity profile of the objects. The distribution of the effective surface brightness as a function of total R -band magnitude is shown in Figure 5. The dashed line indicates the sequence of PSF-size objects in each field. Saturated objects and stars with $R \leq 22$ are removed from this figure.

3.4. Color Classification

We measure the colors of the objects within $2''$ apertures, which corresponds to ~ 0.9 kpc at the Coma Cluster distance. Figure 6 shows the color-magnitude diagram (CMD) of the objects in the Coma Cluster and SDF. Note that only galaxies are plotted for $R \leq 22$ where star/galaxy discrimination was applied, while all the objects are plotted for $R > 22$. The color-magnitude relation (CMR), indicated by the solid line in each panel, is the least-squares fit to all the galaxies in the central region that are spectroscopically confirmed as members of our Coma 1 field from the Mobasher et al. (2001) catalog. It is represented by

$$(B - R) = (-0.029 \pm 0.010)R + (1.55 \pm 0.21), \quad (1)$$

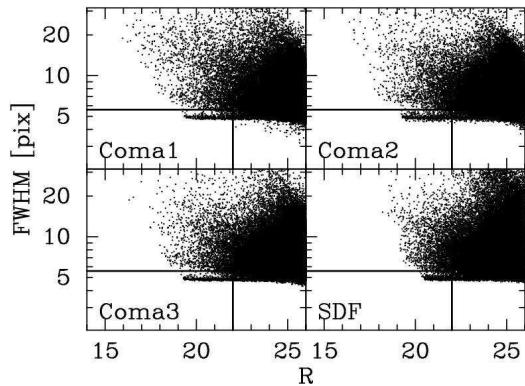


FIG. 4.— FWHM vs. R -magnitude of all objects (excluding saturated objects) in the three observed fields and the SDF. The solid line indicates the discrimination between stars and galaxies. No star/galaxy discrimination is performed at fainter magnitudes ($R > 22$).

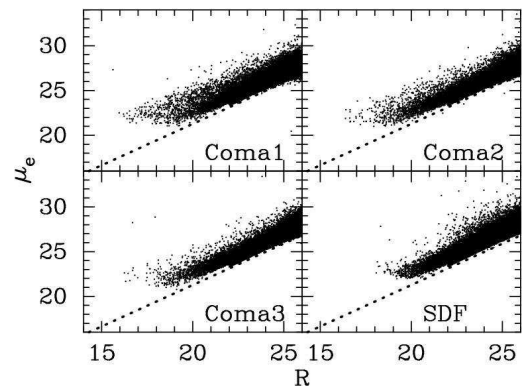


FIG. 5.— The effective surface brightness vs. R -magnitude of objects in the Coma Cluster and the SDF. The sequence of PSF-size objects is shown by the dashed line in each panel. Note that we exclude saturated objects and stars brighter than $R = 22$.

and broadly consistent with the CMR by $(B - R) = (-0.045 \pm 0.028)R + (2.27 \pm 0.48)$ in their bandpass of Adami et al. (2006a).

Adami et al. (2006b) reported that most of the faint galaxies ($21 < R < 25$) follow the CMR derived for brighter elliptical galaxies ($R < 18$) in the Coma Cluster, suggesting that these low-luminosity galaxies experienced a passive evolution similar to brighter ones. Adami et al. (2009) confirmed that the spectroscopically identified dwarf galaxies ($20 < R < 23$) also follow the CMR. Assuming that Equation (1) is valid down to our limiting magnitude ($R \sim 26$), we divide the galaxies into red and blue populations. We adopt the separation boundary which is parallel to the CMR but shifted blueward by $\Delta(B - R) = -0.2$, i.e., $(B - R) = -0.029R + 1.35$.

3.5. Completeness and False Detection Estimate

Detection completeness of objects in the Suprime-Cam images depends on the object magnitudes. We estimate the completeness through a series of simulations by detecting artificial objects in the original images following the procedure given in Kashikawa et al. (2004). Gaussian profiles with different peaks whose FWHM is equal to the seeing size are given to artificial objects. These artificial objects are randomly distributed on the object-subtracted image, which is `-OBJECTS` check image made by SExtractor. We mask circular areas around objects

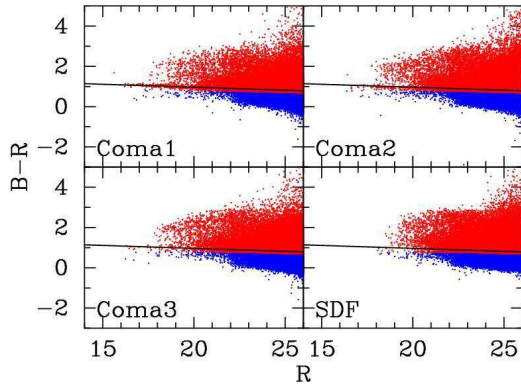


FIG. 6.— Color magnitude diagram ($B - R$ vs. R) in the Coma Cluster and the SDF. The solid line in each panel represents the color magnitude relation of bright galaxies in our Coma 1 region. We separate red and blue galaxies based on the line shifted blueward by $\Delta(B - R) = -0.2$.

with $> 10\sigma$ detection threshold of the sky background noise on the image to avoid detections of artificial objects embedded above bright objects. The radius of each circle is $\text{FWHM} \times 1.5$ of these bright objects. The artificial star magnitudes are distributed every 0.5 mag from 20.0 mag to 27.0 mag. We extract the artificial objects with SExtractor using exactly the same parameters as in §3.3, and estimate the completeness factor, $k(R)$, i.e., the number of the detected objects divided by the number of artificial objects in the input list as a function of R magnitude. We generate 250 artificial objects for each magnitude bin and repeat the process ten times. The detection completeness for our catalog is shown by the solid curves in Figure 7. Each image has more than 90% completeness at $R < 23.5$.

We also show the false detection rate for R -band detected objects by the broken curves in Figure 7. It is estimated by performing photometry on the negative image at the same threshold level as the positive i.e. observed image using the SExtractor. We confirm that the false detection rate is almost 0% down to $R = 25$ in all fields. Therefore, no correction of the false detection rate is performed in this study.

We use observed galaxies down to $R = 25$ ($M_R = -10$) and perform the completeness correction by calculating $N(R)_{\text{corrected}} = N(R)_{\text{observed}}/k(R)$ for each 0.5 magnitude bin. The magnitude error of artificial objects between input and output magnitudes is less than 0.05 mag at $R = 25$ in all images.

4. CONSTRUCTING LUMINOSITY FUNCTION

4.1. Number Density

First, we derive the number density of all the objects and red and blue objects as a function of R magnitude applying the completeness correction. Figure 8 shows the number density of all the objects while Figure 9 shows that of red and blue objects in the three fields of the Coma Cluster and the SDF. The error bars show the Poisson errors.

4.2. Subtraction of Background/Foreground Galaxies

The LF is defined as the number density of galaxies per unit magnitude interval as a function of absolute magnitude: $dN(M) = \phi(M)dM$, where $dN(M)$ is the number of galaxies per unit area with magnitudes in the M to

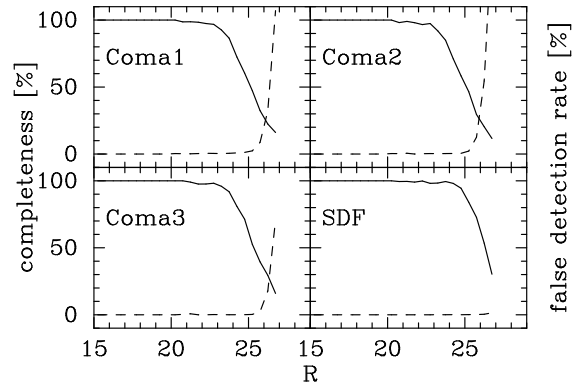


FIG. 7.— The detection completeness (solid line) and the false detection rate (broken line) for the Coma Cluster and the SDF as a function of R -band magnitude.

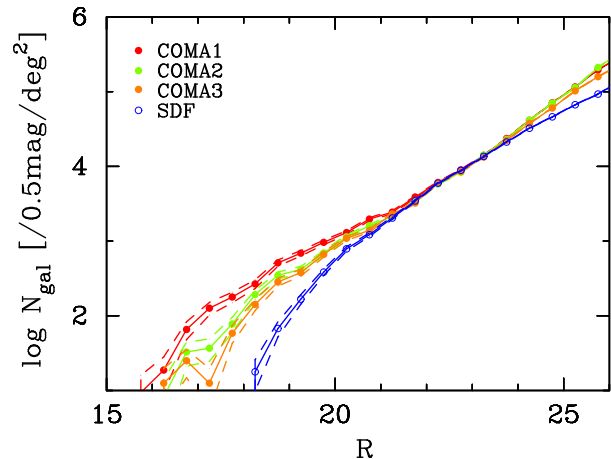


FIG. 8.— The number density of all the objects in the Coma Cluster and the SDF plotted against R -band magnitude. All counts are scaled to an area of 1.0 deg^2 and the completeness corrections are performed. The Poisson statistical errors are shown as dashed lines.

$M + dM$ range. To derive the intrinsic LFs of cluster galaxies, we must correct for the effect of contaminant galaxies, which are mainly located behind the cluster.

We use the statistical background subtraction method (e.g. de Propris et al. 1995; Bernstein et al. 1995; Phillipps et al. 1998; Trentham 1998; Kambas et al. 2000; Yagi et al. 2002b; Popesso et al. 2005; Milne et al. 2007). We perform the subtraction using the surface brightness versus magnitude diagram shown in Figure 5. We divide the diagram into meshes with $\Delta\mu_e = 1.0 \text{ mag arcsec}^{-2}$ and $\Delta R = 0.5 \text{ mag}$ and denote the number of objects in a mesh as $N(\mu_e, R)$. The number density of member galaxies is given by:

$$N(\mu_e, R)_{\text{mb}} = N(\mu_e, R)_{\text{cl}}/k_1(R) - N(\mu_e, R)_{\text{f}}/k_2(R), \quad (2)$$

where $N(\mu_e, R)_{\text{mb}}$ is the number density of member galaxies of the cluster per unit area (1.0 deg^2), $N(\mu_e, R)_{\text{cl}}$ is the number density of all the objects obtained from a cluster field, and $N(\mu_e, R)_{\text{f}}$ is the number density of all the objects obtained from the SDF, the control field. Here, $k_1(R)$ and $k_2(R)$ are the completeness factors for the cluster field and control field, respectively (Figure 7). This procedure is applied to each of the three Coma fields in computing the number density of all the objects and

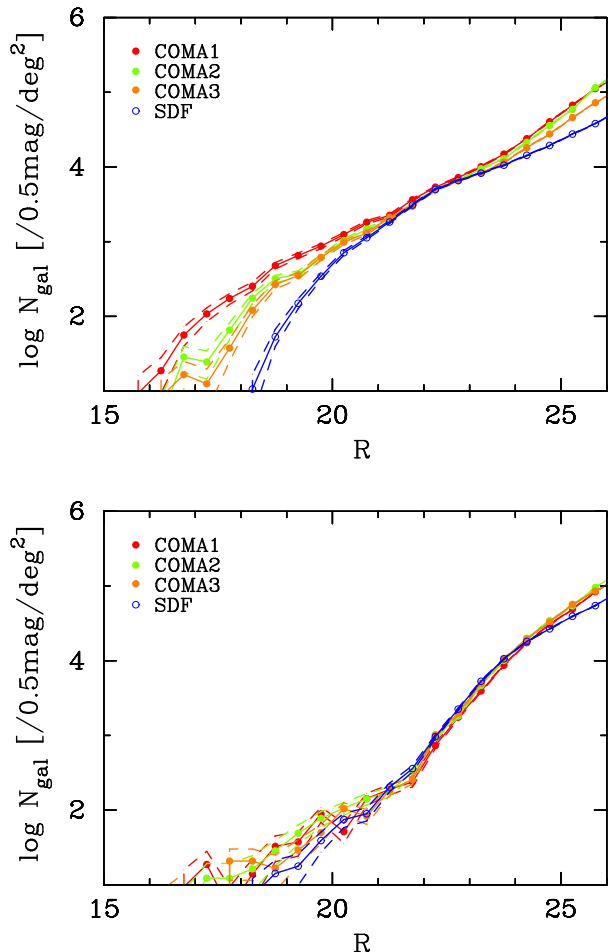


FIG. 9.— The number density of red (*top*) and blue (*bottom*) objects in the Coma Cluster and the SDF plotted against R -band magnitude. The color separation is based on the CMR of the Coma 1 region (for details in §3). All counts are scaled to an area of 1.0 deg^2 and the completeness corrections are performed. The Poisson statistical errors are shown as dashed lines.

red and blue objects. After the statistical subtraction, we summed up $N(\mu_e, R)_{\text{mb}}$ with respect to μ_e to obtain the LF of the cluster $N(R)_{\text{mb}}$.

4.3. The Effect of Cosmic Variance

In order to check the effect of cosmic variance on the LF, we re-compute the Coma LF using the SXDS as the alternative control field. The SXDS is composed of five sub-fields which are referred to as Center, North, South, East and West. Each of the SXDS fields has the same size of field of view as the SDF and the Coma fields. However, the SXDS fields are located at a lower Galactic latitude than the SDF and the Coma fields ($b \sim 88^\circ$ for Coma, $b \sim 83^\circ$ for SDF, $b \sim -60^\circ$ for SXDS).

We show in Figure 10 the LFs in the three regions of the Coma Cluster estimated by the statistical background subtraction using the five SXDS fields as the control field. The errors of each LF are estimated based on Poisson statistics. Figure 10 indicates that the error bars of all LFs overlap in the whole magnitude bins in all Coma fields. When the LFs reach the magnitude of $R \sim -13$, their slopes change. The two clear components (bright component and faint component) of different slopes are confirmed in all the LFs. We conclude that

the effect of cosmic variance is insignificant between the SDF and the SXDS fields. In the SXDS-South region, some massive structures with masses close to $10^{14} M_\odot$ were discovered by Finoguenov et al. (2010). From their results, the SXDS-North region is not polluted by background massive structures. We made the LF shown in Figure 10 without masking the massive structure in the SXDS-South. We do not see any significant effect of the structure.

In this paper, we adopt the LFs obtained by using the SDF as the control field because the SDF and the Coma Cluster are located at nearly the same Galactic latitude, and the number count of faint stars are similar to the two fields.

4.4. Contribution from Globular Clusters

At faint magnitudes, we must consider the contamination from globular clusters (GCs). Unresolved low-luminosity galaxies whose angular sizes are similar to the seeing size cannot be distinguished from bright GCs that appear as point sources at the distance of the Coma Cluster. One of the fundamental parameters of GC study is the specific frequency (Harris & van den Bergh 1981)

$$S_N = N_{GC} 10^{0.4(M_V + 15)}, \quad (3)$$

where N_{GC} is the total number of GCs in the galaxy. S_N is normalized to a galaxy with an absolute V magnitude of -15 . Marín-Franch & Aparicio (2002) studied the GCs of 17 elliptical galaxies in the Coma Cluster and found a mean value of the specific frequency $S_N = 5.1$. On the other hand, the GC luminosity function (GCLF hereafter) of a galaxy is described by a Gaussian distribution function (Harris 1991):

$$n_{GC}(m) = \frac{N_{GC}}{\sqrt{2\pi}\sigma} e^{-(m-m^0)^2/2\sigma^2}, \quad (4)$$

where N_{GC} is the total number of GCs, m^0 is the turnover (peak) magnitude of the distribution, and σ is the dispersion. Harris et al. (2009) reports the GCLF parameters for giant elliptical galaxies in the Coma Cluster as $V^0 = 27.7$ and $\sigma = 1.48$. We compute the total GCLF around giant red galaxies brighter than $M_R = -18$ in the Coma 1 field based on Equations (3) and (4). The GC contamination from galaxies fainter than $M_R = -18$ is much smaller than from giant galaxies. No separate estimation of the total GCLFs is performed in Coma 2 and Coma 3 fields since the total GCLFs in these fields are supposed to be below that in the Coma 1 field.

5. RESULTS

5.1. Luminosity Function of All Galaxies

The top panel of Figure 11 shows the LF of all the three fields while the bottom panel shows the LFs of Coma 1, 2, and 3 fields separately. The broken curve in Figure 11 is the total GCLF of the Coma 1 field computed in §4.4. From Figure 11, we find that the faintest part of the LF ($M_R > -12$) remains nearly unaffected by GCs ($< 15\%$) because the number of faint dwarf galaxies at $M_R > -12$ is about 10 times larger than that of GCs even in the Coma 1. Peng et al. (2011) observed that intracluster GCs in the Coma Cluster have a flat spatial distribution within 520 kpc from NGC 4874. The number

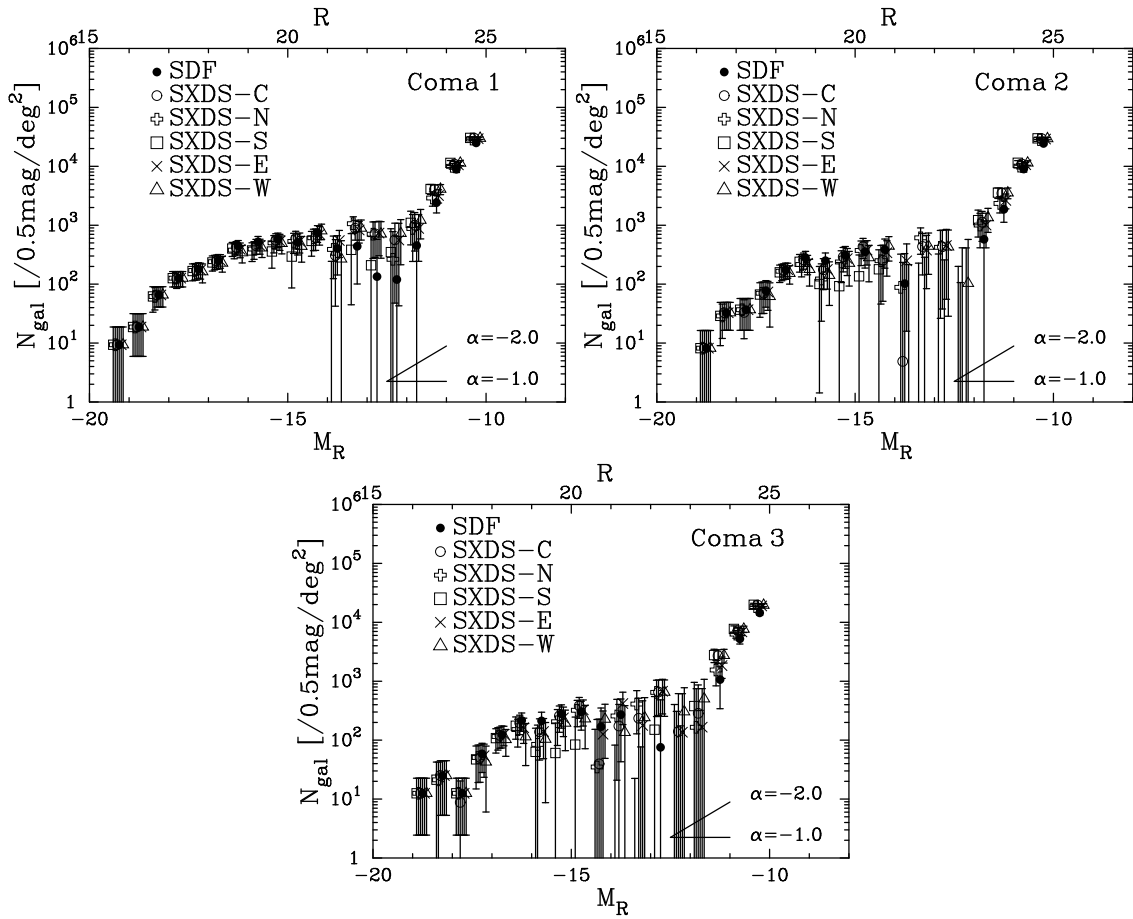


FIG. 10.— The LFs in the Coma 1 (*top-left*), the Coma 2 (*top-right*) and the Coma 3 (*bottom*) obtained by the statistical background subtraction using different control fields, the SDF and the five SXDS fields. Note that each of the five SXDS fields is indicated by center (C), north (N), south (S), east (E) and west (W), respectively. The error bars of the LFs come from the Poisson statistics.

count of intracluster GCs at $r = 520$ kpc is less than 1% of that of GCs around NGC 4874, and it is considered to be negligible. Furthermore, we masked the regions around giant galaxies on our images as mentioned in §3.3. Indeed, at least more than 50% of the total number of GCs around these galaxies are excluded from our data, if we refer to Harris et al. (2009). Therefore, the GCLF shown by the broken curve in Figure 11 can be regarded as the upper limit of the GC contaminations for both the total LF and for each LF of the three fields.

The top panel shows the clear signature of two components comprising the faint part of the LF. One is dominant at $-19 < M_R < -13$ and the other is dominant at $-13 < M_R < -10$. They are hereafter referred to as the bright dwarf component (BDC) and the faint dwarf component (FDC), respectively. These distinct components appear in all the LFs in spite of the different environments such as the Coma 1, 2 and 3. No significant difference is found in the *shape* of the LF among the three regions.

Mobasher et al. (2003) reported that the bright part of the LF ($-23 < M_R < -16$) is similar in the central and outer regions (including our Coma 2 and Coma 3 fields). On the other hand, Adami et al. (2007a) indicated in their Figure 11 that small-scale spatial variations of the LF exist in the regions surrounding giant galaxies in the center of the Coma Cluster. They divided their observed area ($\sim 0.5 \text{ deg}^2$) into 20 subregions of ($10' \times 10'$) and

examined the LFs of the objects in the subregions. In this study we are interested in the possible variation of the LF over much larger spatial scale than that examined by Adami et al. (2007a), i.e., global scale represented in terms of the core, intermediate, and outskirts of the cluster. In this context, we conclude that the *shape* of the LF is very similar in the cluster regardless of the field location over the very wide magnitude range so far investigated ($-23 < M_R < -10$).

The characteristic magnitude of the best-fit Schechter function (Schechter 1976) to Coma galaxies is $M_R^* \sim -20.5$ (Mobasher et al. 2003). Since most of our galaxies are much fainter than this magnitude, we quantify our LFs with the logarithmic slope α which is represented, as in Andreon & Cuillandre (2002), by

$$\alpha = -\frac{1}{0.4} \frac{\partial \log \phi}{\partial M} - 1, \quad (5)$$

In practice, we derive α by the linear regression method as

$$\log \phi = -0.4(\alpha + 1)M + \text{const.} \quad (6)$$

not by fitting the Schechter function to the LF.

The fitting procedures are performed for the whole range of $-19 < M_R < -10$, and for the BDC and for the FDC, separately. We summarize the derived slopes α in Table 3. Although slopes of the three fields differ slightly, they are consistent within errors. The FDC has a

	whole	BDC	FDC
Field	$-19 < M_R < -10$	$-19 < M_R < -13$	$-13 < M_R < -10$
Coma 1	-1.77 ± 0.04	-1.58 ± 0.14	-3.38 ± 0.28
Coma 2	-1.89 ± 0.05	-1.73 ± 0.22	-3.58 ± 0.25
Coma 3	-1.84 ± 0.07	-1.54 ± 0.25	-3.60 ± 0.42

TABLE 3
LIST OF THE FAINT-END SLOPE α IN EACH LF FOR R -BAND.

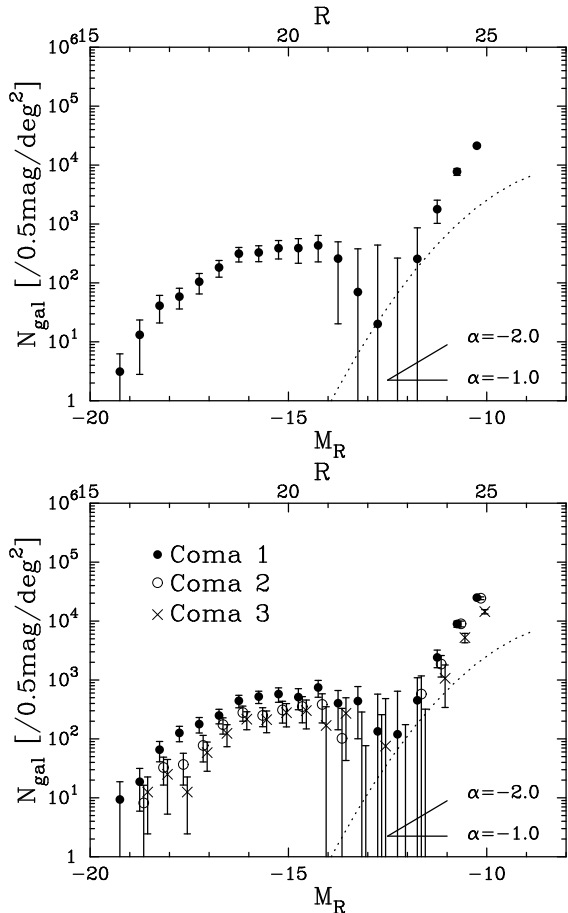


FIG. 11.— *Top*: the total R -band LF of Coma 1, Coma 2 and Coma 3. *Bottom*: the LFs of the Coma 1 (filled circles), Coma 2 (open circles) and Coma 3 (cross marks) fields, respectively. The error bars are based on Poisson statistics. The broken curve indicates the LF of GCs in the Coma 1 field calculated using the previous results of Marín-Franch & Aparicio (2002) and Harris et al. (2009). All counts are scaled to an area of 1.0 deg^2 . Note that the LF plots of Coma 2 and Coma 3 are shifted rightward for the visibility.

much steeper slope ($\alpha < -3$) than the BDC ($\alpha \sim -1.6$).

We did not perform star/galaxy separation below the limit of $R = 22$ where many of our galaxies are too small to be distinguished from stars or globular clusters (GCs). The counts of Galactic stars fainter than this limit in the Coma Cluster are subtracted statistically using the corresponding star counts in the SDF. Figure 12 shows how the LF of Coma 1 field changes when we adopt different limits. The LFs for $R = 21$, $R = 22$ and $R = 23$ are all within the errors. We discuss the contamination from GCs for details in §4.4.

5.2. Comparison with LFs from Previous Studies

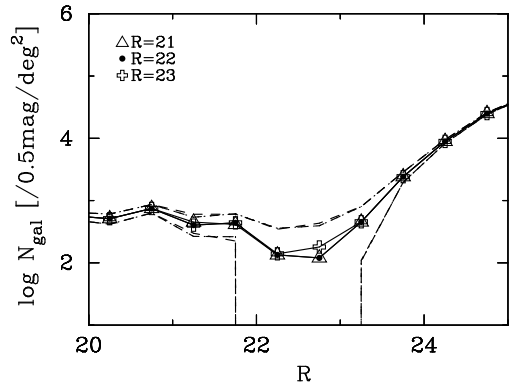


FIG. 12.— The R -band LFs in the Coma 1 (filled circles) when we set the star/galaxy discrimination limit to $R = 21$ (open triangles), $R = 22$ (filled circles) and $R = 23$ (open crosses). The dashed lines indicate errors in Poisson statistics. All counts are scaled to an area of 1.0 deg^2 .

Many observational studies have been performed on the Coma Cluster LFs. The LFs of the Coma Cluster in the R -band from previous studies are shown in Figure 13. Our total LF (red circles) (Coma 1 + Coma 2 + Coma 3) covers an unprecedentedly wide magnitude range.

The LF of our BDC agrees with most of the previous determinations down to $M_R \sim -13$, and the LF of our FDC is broadly consistent with the LFs given by Milne et al. (2007), Bernstein et al. (1995). The LFs from Milne et al. (2007) and Bernstein et al. (1995) are based on observations of a much smaller region in the cluster core. Their effective areas are only $< 5\%$ of the field of our Coma 1 field. Using our wide and deep imaging data, we confirm that the LF in the FDC of the Coma Cluster is rising steeply, similar to the findings of Milne et al. (2007) and Bernstein et al. (1995), at $M_R > -13$. The plots of Adami et al. (2007b) come from the data of their field 2 ($\sim 70 \text{ arcmin}^2$) and it is inconsistent with our result.

Their LF have no clear gap which distinguishes between the BDC and the FDC, although the small dip is found at $M_R \sim -13$. However, their LFs in the central strip region ($\sim 300 \text{ arcmin}^2$) of the Coma Cluster (including the field 2), seems to be strongly dependent on the local environments. Actually, their LF in the field 2 is very different from that in field 1, next to field 2 toward west. The LF of their field 1 has deep dip at $M_R = -13$, and it has no FDC due to the contribution from GCs. The difference between their results and ours may be due to the difference in the size of observed area, i.e., a small area in the cluster core would be susceptible to the effect the local environment associated with the bright cD galaxy. Our LF is consistent with most of the previous results and we show clearly that it is composed of well-defined two components of the BDC and the FDC.

5.3. Properties of BDC and FDC galaxies

First, we investigate the color of dwarf galaxies. Figure 14 shows the LF of red and blue galaxies defined in §3.4 in the three fields. It is clear from Figure 14 that red galaxies are the dominant galaxy population in the BDC of all the three fields. The small fraction of blue galaxies in the BDC ($< 10\%$) is nearly the same in the three fields. On the other hand, the FDC of the Coma 1 is dominated

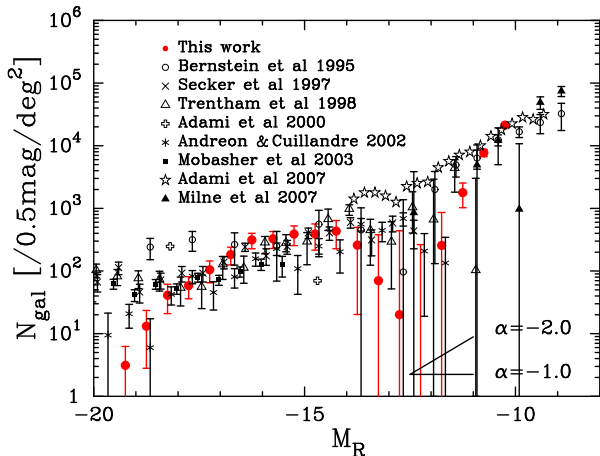


FIG. 13.— The R -band LFs of galaxies in the Coma Cluster from the literature. The red circles indicate our LF in total area of Coma 1, Coma 2 and Coma 3. The ordinate shows logarithmic counts per 0.5 mag bin per deg^2 .

by red galaxies, while those of the Coma 2 and 3 contain some blue galaxies. The fraction of blue galaxies at the faintest magnitude bin ($-11 < M_R < -10$) is $\sim 10\%$ in the Coma 1 field while it is $\sim 40\%$ in the Coma 3 field.

Next, we investigate the relationship between the magnitude and the surface brightness. Figure 15 shows the color-coded density contour map in the magnitude versus surface brightness plane. The left, middle, and right columns are for the Coma 1, Coma 2 and Coma 3 fields, respectively, while the top, middle and bottom rows are for all, red and blue galaxies, respectively. The white line in Figure 15 is the line of star-like objects in Figure 5 shifted upward by $1.0 \text{ mag arcsec}^{-2}$, $\mu_e = 0.93M_R + 36.2$. This line is used here to discriminate between extended (low surface brightness) objects and compact (high surface brightness) objects. We find both extended and compact objects in the Coma 1 field, but very few extended objects are seen in the Coma 2 and Coma 3 fields.

Deep spectroscopic studies of faint galaxies in the Coma Cluster (e.g., Adami et al. 2009; Chiboucas et al. 2010) help us to verify our photometric results derived from the statistical background subtraction. Adami et al. (2009) presented the faint galaxies ($-14 < M_R < -12$) which are spectroscopically confirmed cluster members, follow the CMR of giant member galaxies and their surface brightness spans approximately $2 \text{ mag arcsec}^{-2}$ at $M_R = -13$. In addition, they found that the compact objects are a minor component which represent at most 5% of the member galaxies. This is consistent with our results of Coma 1 of Figure 15. The population of our compact objects is much smaller than that of extended ones down to $M_R = -12$. Also Chiboucas et al. (2010) reported the spectroscopic results of dwarf galaxies ($-16 < M_R < -11$) in the core region of the Coma 1. They examined the galaxy membership in terms of their properties such as morphology, surface brightness, size, and color using 140 dwarf candidates. Their magnitude limit is $M_R = -13$ for the low surface brightness objects and $M_R = -11$ for the high surface brightness objects, while our limit is $M_R = -10$ for both of the low and high surface brightness objects although we have no spectroscopic confirmation. They obtained the confirmed members of about 50 low surface brightness galaxies (LS-

BGs) with magnitudes in the range $-16 < M_R < -13$, and about 20 ultra compact dwarfs (UCDs) in the range $-13 < M_R < -11$. Their results show that the difference of the surface brightness between LSBGs and UCDs is about $2 \text{ mag arcsec}^{-2}$ at $M_R = -13$ (see Figure 13 of Chiboucas et al. 2010). We also find that the difference of the surface brightness between our extended galaxies (objects above the white line in Figure 15) and compact galaxies (objects below the white line in Figure 15) at $M_R = -13$ in the Coma 1 field is about 2 magnitude, consistent with their value. Additionally, the magnitude distributions of their UCDs are also consistent with our compact galaxies.

Our wide field survey revealed the following. Most of BDC galaxies are extended and red. The number of such galaxies increases toward the cluster center. Very few blue extended galaxies are found in all the three fields. On the other hand, FDC galaxies are predominantly compact with sizes (FWHM) comparable to the seeing size, corresponding to $\sim 0.45 \text{ kpc}$ at the distance of the Coma Cluster. Although most of them are red, some are blue. Especially, a lot of blue compact galaxies exist in the FDC of Coma 3 compared to Coma 1. In contrast, almost no extended galaxies is found in the FDC of Coma 3. The extended galaxies of FDC seem to exist only in the dense regions such as the cluster center.

6. DISCUSSIONS

First, we compare our total LF of the Coma Cluster with those of nearby clusters taken from the literature. The slope of the faint part of LF, α , for nearby clusters are summarized in Table 4. Note that we re-computed the values of α for previous studies by fitting Equation (6) to the data values given in respective papers, assuming that $H_0 = 70 \text{ km s}^{-1} \text{ Mpc}^{-1}$, $\Omega_m = 0.3$, and $\Omega_\Lambda = 0.7$. The slopes were derived by fitting in two different magnitude ranges, $-15.0 \leq M \leq -12.5$ and $-12.5 \leq M \leq -10.0$ corresponding to the BDC and the FDC, respectively. The two fitting ranges are fixed regardless of the passbands used. We found that the LF of the Centaurus Cluster is similar to that of the Coma Cluster showing the clear sign of BDC and FDC and similar values of the slopes.

Next, we examine the correlation between the faint-end slope (α) and other cluster properties, i.e., the redshift (z), the Bautz–Morgan type, the velocity dispersion (σ), the X-ray temperature (T_X) and luminosity (L_X). The correlation coefficients between α and the cluster parameters are listed in Table 5. We evaluate the p-value, based on the two-tailed test for the Pearson product-moment correlation coefficient. No significant correlation is confirmed with z , BM type, σ , or L_X for either of the two components, except for a possibly significant correlation with T_X for the FDC ($-12.5 \leq M \leq -10.0$). The slope tends to become steeper for clusters with higher temperatures. The field LF has a much flatter slope ($\alpha \sim -1.3$) than the slope of the cluster LFs (e.g., Trentham et al. 2005; Blanton et al. 2005; Liu et al. 2008). The X-ray temperature is related to the cluster mass (Reiprich & Böhringer 2002; Stanek et al. 2006).

Our comparison and correlation analysis mentioned above have led us to the conjecture that the LF in the cluster is determined by the intrinsic properties and the

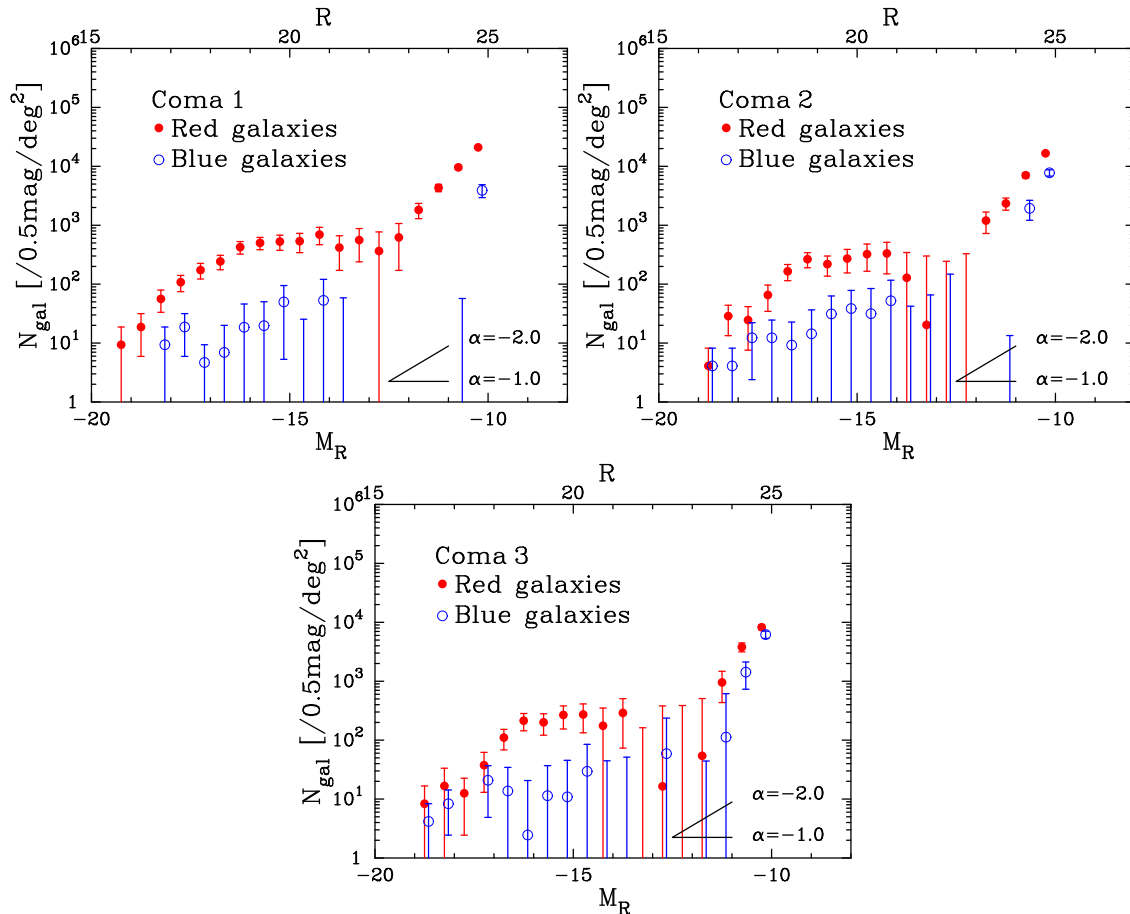


FIG. 14.— The red (*filled red points*) and blue galaxy (*open blue points*) LFs of R -band in each field of the Coma Cluster.

evolutionary stage. Slopes of the BDC and FDC might be related to the cluster global mass. In massive clusters, there is a tendency for galaxies in the BDC to have a flatter LF and for galaxies in the FDC to have a steep one. Such features of the LFs of high-mass clusters may reflect some physical processes that influenced the formation and evolution of dwarf galaxies, such as increased intra-cluster medium pressure, tidal interaction with crossing galaxies, and mergers.

The cold dark matter scenario assumes that dwarf galaxies are formed very early in the Universe. Based on cosmological simulations, Ricotti & Gnedin (2005) and Bovill & Ricotti (2009) showed that dwarf galaxies forming at $z > 6$ were faint dwarf spheroidal galaxies in the present day universe. Their “primordial scenario” has dwarf galaxies starting close to their current stellar mass of about $10^{3-6} M_{\odot}$. Some of these galaxies might be included in the FDC of the Coma Cluster.

We found that colors of dwarf galaxies in the Coma Cluster seem to be related to the environments. A large number of red galaxies are found in the center of the Coma Cluster while they get fewer towards outside. The “tidal stripping scenario” (Mayer et al. 2001; Bournaud & Duc 2006) predicts that low-luminosity galaxies would be formed from more massive gas-rich galaxies. In the center of massive clusters, many tidally disrupted debris of such gas-rich galaxies are produced (Henriques et al. 2008, Bournaud et al. 2008) and their gas is effectively removed by ram pressure strip-

ping (e.g., Gunn & Gott 1972; Farouki & Shapiro 1980; Takeda et al. 1984; Marcolini et al. 2003; Goto 2005; Mori & Burkert 2000). This effect may explain the existence of many red dwarf galaxies in the center of massive clusters.

We also find a large number of compact galaxies, which have comparable sizes to PSF, in all the three observed fields. Recent studies suggest the existence of a number of UCD galaxies in the core of the Coma Cluster (Chiboucas et al. 2010; Madrid et al. 2010). It is natural to assume that the compact population represented in the FDC of the LFs contains the UCDs. Several studies suggest that the UCDs are the remnant nuclei of dwarf elliptical galaxies that have lost their outer parts due to the tidal disruptions during passages close to the central cluster galaxy, in a process called “galaxy threshing” (e.g., Bekki et al. 2003; Mieske et al. 2004; Gregg et al. 2009). Meanwhile the formation of UCDs is linked to the merger of young massive star clusters formed during galaxy mergers (e.g., Fellhauer & Kroupa 2002; Maraston et al. 2004). Thus, major galaxy mergers form a large number of compact stellar objects that are progenitors of GCs and UCDs (Bournaud et al. 2008). Madrid et al. (2010) found that UCD candidates in the Coma Cluster are not only red but also blue. If the UCDs originate from the interactions of galaxies, the faint end of LFs in massive clusters like the Coma Cluster are expected to have steep slopes due to the strong tidal field and frequent galaxy-galaxy mergers.

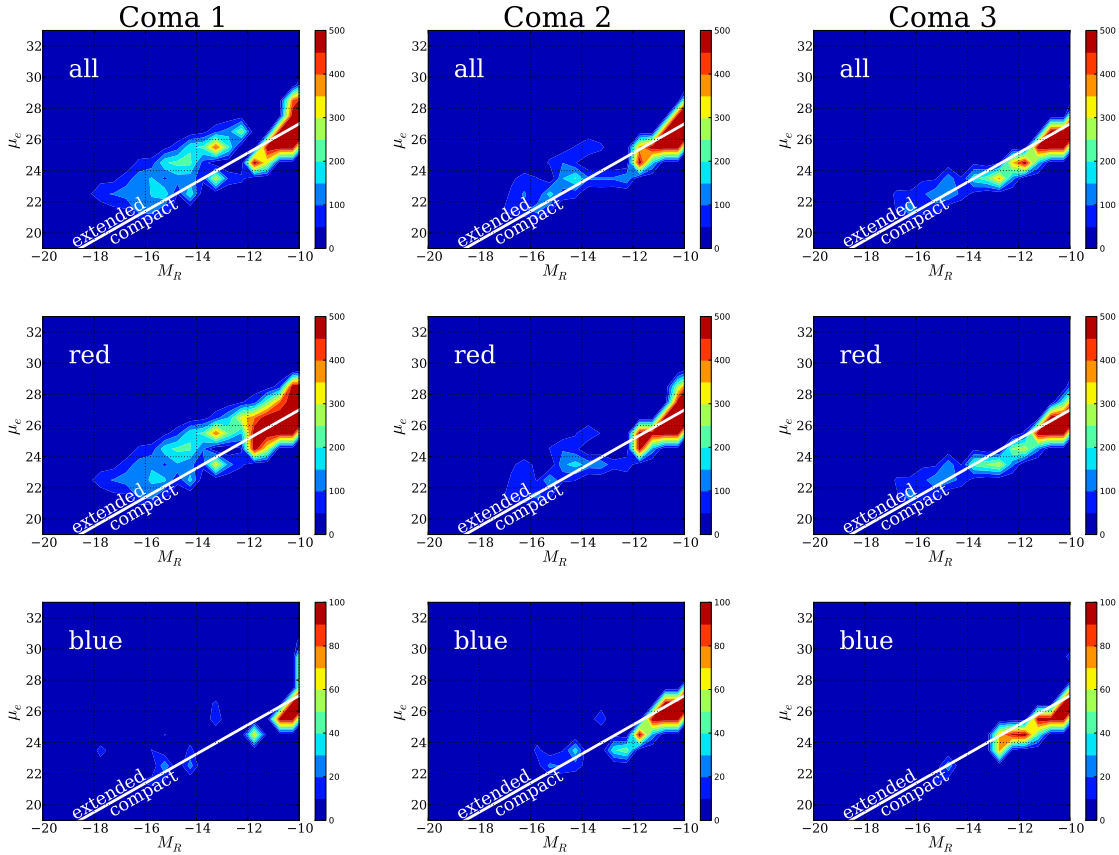


FIG. 15.— The color-coded number density contours of estimated member galaxies (all galaxies: *top row*, red galaxies: *middle row*, blue galaxies: *bottom row*) in the R absolute magnitude versus effective surface brightness plane. Coma 1, Coma 2 and Coma 3 fields are in left, middle and right columns, respectively. The statistical background subtraction is carried out here. The number density in each mesh is normalized to 1.0 deg² and corrected for the detection completeness. The white solid line indicates the discrimination between the extended and the compact objects.

We find that the outskirts contain a large fraction of blue galaxies of $-11 < M_R < -10$ compared to the central region. Smith et al. (2009) found that the passive dwarf galaxies are younger in the outskirts than those in the core of Coma Cluster, and supported the scenario in which many these galaxies are the quenched remnants of infalling late-type galaxies. If late-type dwarf galaxies in clusters were star-forming galaxies infalling from outside, the steep slopes in the blue galaxy LFs and the large number of blue dwarfs in the outskirts of the cluster would be explained.

In summary, the faint part of LF in the Coma Cluster seems to consist of some populations of galaxies whose origins are different. We suggest that these red galaxies contain primordial dwarf galaxies, UCDs of the tidal origin and remnants of disrupted dwarf galaxies, while blue dwarf galaxies contain some blue UCDs and infalling late-type dwarf galaxies from the outer fields. In order to understand their origin, the spectroscopic information such as their dynamics and metallicity is essential. Further investigations, we require the spectroscopic observations of very faint galaxies down to $M = -10$ in various regions of the Coma Cluster to identify member galaxies.

7. CONCLUSIONS

We construct the galaxy luminosity functions (LFs) for the Coma Cluster, the richest of the nearby galaxy clusters. Deep and wide images of the Coma Cluster

are obtained with the Suprime-Cam mounted on the Subaru Telescope. The resultant LFs cover the range of $-19 < M_R < -10$. Contamination from background galaxies is subtracted statistically using the number counts of galaxies in a blank field, the Subaru Deep Field.

Our main results are summarized as follows:

1. We derive LFs in the cluster center region (Coma 1 field), the NGC 4839 group (Coma 2 field) and the outskirts (Coma 3 field). No significant differences in the shape of the LFs are found in the different fields of the Coma Cluster.
2. The faint part of LF in the Coma Cluster contains two distinct components; the bright dwarf component (BDC; $-19 < M_R < -13$) which has a relatively flat LF slope and the faint dwarf component (FDC; $-13 < M_R < -10$) which has a steep slope.
3. Most of BDC galaxies are extended and red. The number of such galaxies increases toward the cluster center. Very few extended and blue galaxies are found in the BDC of all the three fields. The fraction of blue (both extended and compact) galaxies in the BDC ($< 10\%$) is nearly the same in all the three fields.
4. On the other hand, FDC galaxies are predominantly compact with sizes comparable to the see-

Cluster	z	BM	σ (km s ⁻¹)	L_X (10 ⁴⁴ erg s ⁻¹)	T_X (keV)	Band	α		Reference
							(-15 ≤ M ≤ -12.5)	(-12.5 ≤ M ≤ -10.0)	
Virgo	0.0036 ^a	III	643 ^e	0.418 ^g	2.28 ^g	B	-1.61 ± 0.07	-0.56 ± 0.10	Sabatini et al. 2003
	0.0036	III	643	0.418	2.28	B	~ -1.5	~ -1	Trentham & Hodgkin 2002
	0.0036	III	643	0.418	2.28	R	-2.06 ± 0.06	-2.07 ± 0.24	Phillipps et al. 1998
Fornax	0.0046 ^b	I	374 ^f	0.00119 ^h	1.56 ^k	B	~ -2	~ -2	Kambas et al. 2000
	0.0046	I	374	0.00119	1.56	V	-1.38 ± 0.06	-1.26 ± 0.01	Hilker et al. 2003
Centaurus	0.0114 ^c	I-II	863 ^c	1.378 ^h	3.69 ^k	V	-0.69 ± 0.13	-3.73 ± 0.03	Chiboucas & Mateo 2006
Hydra	0.0126 ^c	III	647 ^c	0.569 ^h	3.15 ^k	B	-1.88 ± 0.04	-1.38 ± 0.08	Yamanoi et al. 2007
	0.0126	III	647	0.569	3.15	R	-1.48 ± 0.02	-1.64 ± 0.03	Yamanoi et al. 2007
Perseus	0.0179 ^c	II-III	1324 ^c	15.341 ⁱ	6.42 ^k	B	-1.81 ± 0.04	-1.00 ± 0.02	Conselice et al. 2002
	0.0179	II-III	1324	15.341	6.42	B	-1.53 ± 0.09	-	Penny & Conselice 2008
Coma	0.0231 ^c	II	1008 ^c	7.767 ⁱ	8.25 ^l	B	-1.28 ± 0.03	-3.50 ± 0.18	This work
	0.0231	II	1008	7.767	8.25	R	-0.31 ± 0.12	-3.97 ± 0.05	This work
A2199	0.0302 ^d	I	733 ^c	4.079 ^j	3.99 ^j	B	-2.24 ± 0.09	-1.65 ± 0.51	de Propriis et al. 1995

TABLE 4

LIST OF PARAMETERS OF NEARBY CLUSTERS. NOTE THAT THE MAGNITUDE IS CONVERTED INTO THE AB SYSTEM ADOPTING $H_0 = 70$ KM S⁻¹ MPC⁻¹, $\Omega_m = 0.3$, AND $\Omega_\Lambda = 0.7$. THE L_X AND T_X FROM THE X-RAYS CLUSTERS DATABASE (BAX) ARE SET TO $H_0 = 50$ KM S⁻¹ MPC⁻¹, $\Omega_m = 1.0$.

z: redshift

— ^aEbeling et al. (1998), ^bAbell et al. (1989), ^cStruble & Rood (1999), ^dOegerle & Hill (2001)

BM: Bautz-Morgan type (NED)

σ : velocity dispersion

— ^eZabludoff et al. (1990), ^fDrinkwater et al. (2001)

L_X : X-ray luminosity in the 0.1-0.2 keV band

— ^gMatsumoto et al. (2000), ^hBöhringer et al. (2004), ⁱReiprich & Böhringer (2002), ^jVikhlinin et al. (2009)

T_X : X-ray temperature

— ^kIkebe et al. (2002), ^lArnaud et al. (2001)

α : faint-end slope of LF

parameter	$\alpha(-15 \leq M \leq -12.5)$		$\alpha(-12.5 \leq M \leq -10)$	
	correlation coefficient	p-value	correlation coefficient	p-value
z	0.14	0.64	-0.43	0.16
BM	-0.08	0.79	0.33	0.27
σ	0.32	0.29	-0.34	0.26
$\log(L_X)$	0.23	0.45	-0.31	0.31
T_X	0.49	0.09	-0.61	0.03

TABLE 5

LIST OF CORRELATION COEFFICIENTS BETWEEN α AND THE PARAMETER. NOTE THAT THE P-VALUE UNDER 0.05 IS CONSIDERED SIGNIFICANT.

ing size, FWHM corresponding to ~ 0.45 kpc at the distance of the Coma Cluster. Most of them are red, but some are blue. Especially, a lot of blue compact galaxies exist in the FDC of Coma 3 compared to Coma 1. In contrast, almost no extended galaxies is found in the FDC of Coma 3. The extended galaxies of FDC seem to exist only in the dense regions such as the cluster center.

This study is based on the PhD thesis of the first author which was accepted in 2010 at the Graduate University for Advanced Studies (Sokendai). We are grateful to the staff of the Subaru Telescope for their help. We thank Margaret Milne for providing her Coma LF data, Nobuo Arimoto and Tadayuki Kodama for discussions. We

would like to thank anonymous referee for his/her helpful suggestions. This research has made use of the Subaru Deep Field (SDF) archive, the NASA/IPAC Extragalactic Database (NED), the X-Rays Clusters Database (BAX) and the Digitized Sky Surveys (DSS). Funding for the SDSS and SDSS-II has been provided by the Alfred P. Sloan Foundation, the Participating Institutions, the National Science Foundation, the U.S. Department of Energy, the National Aeronautics and Space Administration, the Japanese Monbukagakusho, the Max Planck Society, and the Higher Education Funding Council for England. The SDSS Web Site is <http://www.sdss.org/>. Data analysis were in part carried out on common use data analysis computer system at the Astronomy Data Center, ADC, of the National Astronomical Observatory of Japan.

REFERENCES

- Abell, G. O., Corwin, H. G., Jr., & Olowin, R. P. 1989, *ApJS*, 70, 1
- Adami, C., Ulmer, M. P., Durret, F., Nichol, R. C., Mazure, A., Holden, B. P., Romer, A. K., & Savine, C. 2000, *A&A*, 353, 930
- Adami, C., Picat, J. P., Savine, C., et al. 2006a, *A&A*, 451, 1159
- Adami, C., et al. 2006b, *A&A*, 459, 679
- Adami, C., Durret, F., Mazure, A., et al. 2007a, *A&A*, 462, 411
- Adami, C., Picat, J. P., Durret, F., Mazure, A., Pelló, R., & West, M. 2007b, *A&A*, 472, 747
- Adami, C., Ilbert, O., Pelló, R., et al. 2008, *A&A*, 491, 681
- Adami, C., Le Brun, V., Biviano, A., et al. 2009, *A&A*, 507, 1225
- Andreon, S., & Cuillandre, J.-C. 2002, *ApJ*, 569, 144
- Arnaud, M., et al. 2001, *A&A*, 365, L67
- Beijersbergen, M., Hoekstra, H., van Dokkum, P. G., & van der Hulst, T. 2002, *MNRAS*, 329, 385
- Bekki, K., Couch, W. J., Drinkwater, M. J., & Shioya, Y. 2003, *MNRAS*, 344, 399
- Bernstein, G. M., Nichol, R. C., Tyson, J. A., Ulmer, M. P., & Wittman, D. 1995, *AJ*, 110, 1507
- Bertin, E., & Arnouts, S. 1996, *A&AS*, 117, 393

- Biviano, A., Durret, F., Gerbal, D., Le Fevre, O., Lobo, C., Mazure, A., & Slezak, E. 1995, *A&A*, 297, 610
- Biviano, A., Durret, F., Gerbal, D., Le Fevre, O., Lobo, C., Mazure, A., & Slezak, E. 1996, *A&A*, 311, 95
- Blanton, M. R., et al. 2003, *ApJ*, 592, 819
- Blanton, M. R., Lupton, R. H., Schlegel, D. J., Strauss, M. A., Brinkmann, J., Fukugita, M., & Loveday, J. 2005, *ApJ*, 631, 208
- Böhringer, H., et al. 2004, *A&A*, 425, 367
- Bournaud, F., & Duc, P.-A. 2006, *A&A*, 456, 481
- Bournaud, F., Bois, M., Emsellem, E., & Duc, P.-A. 2008, *Astronomische Nachrichten*, 329, 1025
- Bovill, M. S., & Ricotti, M. 2009, *ApJ*, 693, 1859
- Chiboucas, K., & Mateo, M. 2006, *AJ*, 132, 347
- Chiboucas, K., Tully, R. B., Marzke, R. O., Trentham, N., Ferguson, H. C., Hammer, D., Carter, D., & Khosroshahi, H. 2010, *ApJ*, 723, 251
- Conselice, C. J., Gallagher, J. S., & Wyse, R. F. G. 2002, *AJ*, 123, 2246
- de Propriis, R., Pritchet, C. J., Harris, W. E., & McClure, R. D. 1995, *ApJ*, 450, 534
- Drinkwater, M. J., Gregg, M. D., & Colless, M. 2001, *ApJ*, 548, L139
- Ebeling, H., Edge, A. C., Böhringer, H., Allen, S. W., Crawford, C. S., Fabian, A. C., Voges, W., & Huchra, J. P. 1998, *MNRAS*, 301, 881
- Farouki, R., & Shapiro, S. L. 1980, *ApJ*, 241, 928
- Fellhauer, M., & Kroupa, P. 2002, *MNRAS*, 330, 642
- Finoguenov, A., Watson, M. G., Tanaka, M., et al. 2010, *MNRAS*, 403, 2063
- Furusawa, H., Kosugi, G., Akiyama, M., et al. 2008, *ApJS*, 176, 1
- Goto, T. 2005, *MNRAS*, 359, 1415
- Gregg, M. D., et al. 2009, *AJ*, 137, 498
- Gunn, J. E., & Gott, J. R., III 1972, *ApJ*, 176, 1
- Gunn, J. E., & Stryker, L. L. 1983, *ApJS*, 52, 121
- Harris, W. E., & van den Bergh, S. 1981, *AJ*, 86, 1627
- Harris, W. E. 1991, *ARA&A*, 29, 543
- Harris, W. E., Kavelaars, J. J., Hanes, D. A., Pritchet, C. J., & Baum, W. A. 2009, *AJ*, 137, 3314
- Henriques, B. M., Bertone, S., & Thomas, P. A. 2008, *MNRAS*, 383, 1649
- Hilker, M., Mieske, S., & Infante, L. 2003, *A&A*, 397, L9
- Ikebe, Y., Reiprich, T. H., Böhringer, H., Tanaka, Y., & Kitayama, T. 2002, *A&A*, 383, 773
- Iye, M., et al. 2004, *PASJ*, 56, 381
- Kambas, A., Davies, J. I., Smith, R. M., Bianchi, S., & Haynes, J. A. 2000, *AJ*, 120, 1316
- Kashikawa, N., et al. 2004, *PASJ*, 56, 1011
- Komiyama, Y., et al. 2002, *ApJS*, 138, 265
- Kubo, J. M., Stebbins, A., Annis, J., Dell'Antonio, I. P., Lin, H., Khiabani, H., & Frieman, J. A. 2007, *ApJ*, 671, 1466
- Liu, C. T., Capak, P., Mobasher, B., Paglione, T. A. D., Rich, R. M., Scoville, N. Z., Tribiano, S. M., & Tyson, N. D. 2008, *ApJ*, 672, 198
- Madrid, J. P., et al. 2010, *ApJ*, 722, 1707
- Maraston, C., Bastian, N., Saglia, R. P., Kissler-Patig, M., Schweizer, F., & Goudfrooij, P. 2004, *A&A*, 416, 467
- Marcolini, A., Brighenti, F., & D'Ercole, A. 2003, *MNRAS*, 345, 1329
- Marín-Franch, A., & Aparicio, A. 2002, *ApJ*, 568, 174
- Matsumoto, H., Tsuru, T. G., Fukazawa, Y., Hattori, M., & Davis, D. S. 2000, *PASJ*, 52, 153
- Mayer, L., Governato, F., Colpi, M., Moore, B., Quinn, T., Wadsley, J., Stadel, J., & Lake, G. 2001, *ApJ*, 547, L123
- Mieske, S., Hilker, M., & Infante, L. 2004, *A&A*, 418, 445
- Milne, M. L., Pritchet, C. J., Poole, G. B., Gwyn, S. D. J., Kavelaars, J. J., Harris, W. E., & Hanes, D. A. 2007, *AJ*, 133, 177
- Miyazaki, S., et al. 2002, *PASJ*, 54, 833
- Mobasher, B., et al. 2001, *ApJS*, 137, 279
- Mobasher, B., et al. 2003, *ApJ*, 587, 605
- Mori, M., & Burkert, A. 2000, *ApJ*, 538, 559
- Neumann, D. M., et al. 2001, *A&A*, 365, L74
- Oegerle, W. R., & Hill, J. M. 2001, *AJ*, 122, 2858
- Ouchi, M., et al. 2004, *ApJ*, 611, 660
- Peng, E. W., et al. 2011, *ApJ*, 730, 23
- Penny, S. J., & Conselice, C. J. 2008, *MNRAS*, 383, 247
- Phillipps, S., Parker, Q. A., Schwartzberg, J. M., & Jones, J. B. 1998, *ApJ*, 493, L59
- Poposo, P., Böhringer, H., Romaniello, M., & Voges, W. 2005, *A&A*, 433, 415
- Reiprich, T. H., Böhringer, H. 2002, *ApJ*, 567, 716
- Ricotti, M., & Gnedin, N. Y. 2005, *ApJ*, 629, 259
- Sabatini, S., Davies, J., Scaramella, R., Smith, R., Baes, M., Linder, S. M., Roberts, S., & Testa, V. 2003, *MNRAS*, 341, 981
- Sandage, A., Binggeli, B., & Tammann, G. A. 1985, *AJ*, 90, 1759
- Schechter, P. 1976, *ApJ*, 203, 297
- Schlegel, D. J., Finkbeiner, D. P., & Davis, M. 1998, *ApJ*, 500, 525
- Secker, J., Harris, W. E. & Plummer, J. D. 1997, *PASP*, 109, 1377
- Smith, R. J., Lucey, J. R., Hudson, M. J., Allanson, S. P., Bridges, T. J., Hornschemeier, A. E., Marzke, R. O., & Miller, N. A. 2009, *MNRAS*, 392, 1265
- Stanek, R., Evrard, A. E., Böhringer, H., Schuecker, P., & Nord, B. 2006, *ApJ*, 648, 956
- Struble, M. F., & Rood, H. J. 1999, *ApJS*, 125, 35
- Takeda, H., Nulsen, P. E. J., & Fabian, A. C. 1984, *MNRAS*, 208, 261
- Trentham, N. 1998, *MNRAS*, 293, 71
- Trentham, N., & Hodgkin, S. 2002, *MNRAS*, 333, 423
- Trentham, N., Sampson, L., & Banerji, M. 2005, *MNRAS*, 357, 783
- Vikhlinin, A., et al. 2009, *ApJ*, 692, 1033
- Yagi, M., Kashikawa, N., Sekiguchi, M., Doi, M., Yasuda, N., Shimasaku, K., & Okamura, S. 2002a, *AJ*, 123, 66
- Yagi, M., Kashikawa, N., Sekiguchi, M., Doi, M., Yasuda, N., Shimasaku, K., & Okamura, S. 2002b, *AJ*, 123, 87
- Yagi, M., et al. 2010, *AJ*, 140, 1814
- Yamanoi, H., et al. 2007, *AJ*, 134, 56
- Zabludoff, A. I., Huchra, J. P., & Geller, M. J. 1990, *ApJS*, 74, 1